Europ. J. Agronomy 55 (2014) 89–99

Contents lists available at ScienceDirect

European Journal of Agronomy

journal homepage: www.elsevier.com/locate/eja

Tree height quantification using very high resolution imagery acquired from an unmanned aerial vehicle (UAV) and automatic 3D photo-reconstruction methods

P.J. Zarco-Tejada[a,b,*], R. Diaz-Varela[a,c], V. Angileri[a], P. Loudjani[a]

[a] European Commission, Joint Research Centre, Institute for Environment and Sustainability, Via E. Fermi 2749, I-21027 Ispra, VA, Italy
[b] Instituto de Agricultura Sostenible (IAS), Consejo Superior de Investigaciones Científicas (CSIC), Córdoba, Spain
[c] Department of Botany, GI-1934-TB, IBADER, University of Santiago de Compostela, Escola Politécnica Superior, Campus Universitario s/n, E-27002 Lugo, Spain

ARTICLE INFO

Article history:
Received 27 June 2013
Received in revised form 21 January 2014
Accepted 27 January 2014

Keywords:
DSM
Low-cost camera
Remote sensing
Tree height
Photo reconstruction
3D image modeling

ABSTRACT

This study provides insight into the assessment of canopy biophysical parameter retrieval using passive sensors and specifically into the quantification of tree height in a discontinuous canopy using a low-cost camera on board an unmanned aerial vehicle (UAV). The UAV was a 2-m wingspan fixed-wing platform with 5.8 kg take-off weight and 63 km/h ground speed. It carried a consumer-grade RGB camera modified for color-infrared detection (CIR) and synchronized with a GPS unit. In this study, the configuration of the electric UAV carrying the camera payload enabled the acquisition of 158 ha in one single flight. The camera system made it possible to acquire very high resolution (VHR) imagery (5 cm pixel^{-1}) to generate ortho-mosaics and digital surface models (DSMs) through automatic 3D reconstruction methods. The UAV followed pre-designed flight plans over each study site to ensure the acquisition of the imagery with large across- and along-track overlaps (i.e. >80%) using a grid of parallel and perpendicular flight lines. The validation method consisted of taking field measurements of the height of a total of 152 trees in two different study areas using a GPS in real-time kinematic (RTK) mode. The results of the validation assessment conducted to estimate tree height from the VHR DSMs yielded R^2 = 0.83, an overall root mean square error (RMSE) of 35 cm, and a relative root mean square error (R-RMSE) of 11.5% for trees with heights ranging between 1.16 and 4.38 m. An assessment conducted on the effects of the spatial resolution of the input images acquired by the UAV on the photo-reconstruction method and DSM generation demonstrated stable relationships for pixel resolutions between 5 and 30 cm that rapidly degraded for input images with pixel resolutions lower than 35 cm. RMSE and R-RMSE values obtained as a function of input pixel resolution showed errors in tree quantification below 15% when 30 cm pixel^{-1} resolution imagery was used to generate the DSMs. The study conducted in two orchards with this UAV system and the photo-reconstruction method highlighted that an inexpensive approach based on consumer-grade cameras on board a hand-launched unmanned aerial platform can provide accuracies comparable to those of the expensive and computationally more complex light detection and ranging (LIDAR) systems currently operated for agricultural and environmental applications.

1. Introduction

Canopy height is an important parameter required for inventory, monitoring, and modeling activities (Selkowitz et al., 2012). In particular, it is an ecological measure that provides essential information related to ecological, hydrological, biophysical, micrometeorological, and agronomic processes in natural vegetation and agricultural crops. However, existing spatial datasets provide little information on canopy height. An accurate and automatic estimation of tree height is also important for the identification and monitoring of certain features of agricultural lands in the framework of the European common agricultural policy (CAP). In this regard, since 2005 farmers have had to comply with common rules and standards regarding the environment as well as public, animal

Abbreviations: AAT, automatic aerial triangulation; AGL, above ground level; AHRS, attitude heading reference system; ALS, airborne laser scanner; BBA, bundle block adjustment; CAP, common agricultural policy; CIR, color-infrared; COTS, commercial off-the-shelf; DSM, digital surface model; EFA, ecological focus areas; GAEC, good agricultural and environmental condition; GPS, global positioning system; GSD, ground sampling distance; LIDAR, light detection and ranging; MAMSL, meters above mean sea level; MVS, mutiview-stereo; NDVI, normalized difference vegetation index; RGB, red-green-blue; RMSE, root mean square error; R-RMSE, relative root mean square error; RTK, real-time kinematic; SfM, structure-from-motion; TOW, take-off weight; UAV, unmanned aerial vehicle; VHR, very high resolution.

* Corresponding author at: Instituto de Agricultura Sostenible (IAS), Consejo Superior de Investigaciones Científicas (CSIC), Córdoba, Spain. Tel.: +34 957499280; fax: +34 957499252.
E-mail address: pablo.zarco@csic.es (P.J. Zarco-Tejada).

1161-0301/$ – see front matter © 2014 Elsevier B.V. All rights reserved.
http://dx.doi.org/10.1016/j.eja.2014.01.004

and plant health and animal welfare in order to obtain full 'single farm payments.' Such standards are known as 'cross-compliance' (Council Regulation EC No. 73/2009). As a component of cross compliance, farmers are obliged to keep the agricultural land in good agricultural and environmental condition (GAEC) by respecting a number of minimum requirements in issues such as the prevention of soil erosion, the conservation of soil organic matter and structure, and the maintenance of habitats and landscape features. Further measures are under discussion in the proposal of the 'greening' of direct payments, which may require the need for identifying and characterize landscape features.

One of the measures proposed for the 'greening' of payments establishes that farmers shall ensure that a certain amount of their agricultural land is kept as 'ecological focus areas' (EFA), which refers to a set of elements that delivers environmental benefits. Several types of landscape features such as hedges and trees, either in groups or isolated, are among the elements taken into account in both the GAEC and the EFA proposals. All these elements generally show a distinct contrast in their dimensions and physiognomy (i.e. height) with their surrounding agricultural matrix. Therefore, the estimation of their height is a key input for their automatic identification and monitoring (Bork and Su, 2007), particularly in cases where the spectral responses of landscape features and surrounding crops are often similar. In this regard, the standard multispectral indices currently obtained from passive remote sensors, such as the normalized difference vegetation index (NDVI) calculated from near infrared and red spectral regions (Rouse et al., 1974), are quite limited for mapping vegetation canopy height. This is because reflectance data are primarily sensitive to canopy cover and vegetation density rather than height and thus can only capture canopy height indirectly (Chopping et al., 2008).

For this reason, remote quantification of canopy structural parameters such as canopy height must rely on the development of very high resolution digital models to enable the identification and retrieval of the height of each single tree crown or canopy plot. Such standard methodologies used for the generation of digital surface models (DSMs) usually focus on photogrammetric methods and more recently on the use of active sensors such as light detection and ranging (LIDAR) laser scanners. Both require expensive cameras, well-trained personnel, and precise technology to obtain accurate results. Several examples can be found in the literature regarding the retrieval of canopy height using multi-angle/multi-view passive imagery from both airborne platforms (Waser et al., 2008; Wallerman et al., 2012) and satellite platforms (Takahashi et al., 2012) and also from active laser systems (Kaartinen et al., 2012). In a study, researchers obtained 34% error when retrieving canopy height from aerial DMC imagery in a forest area (Wallerman et al., 2012). Other authors obtained errors ranging between 0.09 m and 1.2 m (i.e. from over 5% to over 10%) when estimating individual tree height from an airborne laser scanner (ALS) (Kaartinen et al., 2012; Ma et al., 2012; Edson and Wing, 2011; Pirotti, 2010; Tesfamichael et al., 2010a,b; Gratziolis et al., 2010). Depending on the segmentation methodology used to process the ALS data, reported errors when quantifying individual tree height ranged between 0.09 and 0.56 m, depending on the type of forest canopy under study such as young conifers and forested plots (Edson and Wing, 2011). Nevertheless, we are not aware of the existence of any other studies on canopy height quantification using very high resolution DSMs obtained from passive sensors.

New progress in the miniaturization and cost reduction of GPS devices, embedded computers, and inertial sensors has opened new possibilities for remote sensing applications using commercial off-the-shelf (COTS) instrumentation (Berni et al., 2009a). Such miniaturization has provided high flexibility in terms of potential applications based on the development of unmanned aerial vehicles (UAVs). In fact, recent studies have demonstrated the feasibility of conducting quantitative remote sensing for vegetation monitoring using miniaturized thermal cameras on board lightweight UAV platforms (Berni et al., 2009a,b; González-Dugo et al., 2012), acquiring narrow-band multispectral imagery (Zarco-Tejada et al., 2009; Suárez et al., 2010; Guillén-Climent et al., 2012), and using micro-hyperspectral imagery for crop stress detection (Zarco-Tejada et al., 2012, 2013a,b).

Nevertheless, miniaturized cameras installed on board unmanned vehicles are usually a compromise between size, weight, specifications, and cost. They tend to produce poorer quality imagery than the metric systems generally used on board manned aircraft with regard to radiometric integrity, sensor signal-to-noise characteristics, and optical geometry deformations. For this reason, specific methodologies are required to perform image calibration and corrections when the aim is to derive accurate remote sensing products from low-cost cameras operated from lightweight platforms. In fact, the use of consumer-grade cameras for field operations and for use on board UAVs has generated a promising research avenue regarding the development of very high resolution DSMs. Structure-from-motion (SfM) and mutiview-stereo (MVS) algorithms are the methods generally proposed when consumer-grade cameras are used as opposed to expensive laser scanners and rigorous photogrammetric methods that require high expertise (Küng et al., 2011).

The assessment of traditional photogrammetric methods as compared to SfM and MVS algorithms has demonstrated comparable results and an 80% time reduction in data collection when applied to 3D reconstruction of surfaces and topography using consumer-grade SLR cameras (James and Robson, 2012). In other studies, researchers have compared MVS algorithms against LIDAR data as a reference for benchmarking camera calibration methods (Strecha et al., 2008) or performed such comparisons using data obtained from consumer-grade camera installed on board lightweight UAVs (Vallet et al., 2011). In such studies, cheap cameras on board ultra-light UAV platforms with a take-off weight under 1 kg generated DSMs with errors below 15 cm using multi-angle correlation methods when compared to a reference digital model.

In this study we explored the use of low-cost UAV imagery and automatic DSM generation methods for canopy height quantification using an inexpensive non-metric consumer-grade color infrared (CIR) camera. We assessed the spatial resolution effects of the VHR imagery used as input for the DSMs generated through automatic processing methods in the context of tree height quantification in orchard fields.

2. Materials and methods

2.1. Study site description and airborne campaigns

The study was performed in an area of 148 ha planted with olive orchards (*Olea europaea* L.) in Alcolea, Cordoba, southern Spain (37° 44′ N, 4° 36′ W, altitude 150 MAMSL) in summer 2012. The area comprised orchards with various canopy densities cultivated either in rows or in patterns and had a gradient in tree crown sizes and heights, as required for the validation methods conducted (Fig. 1).

The airborne campaigns were conducted in summer 2012 using an unmanned aerial vehicle (UAV) operated by the Laboratory for Research Methods in Quantitative Remote Sensing (QuantaLab, IAS-CSIC, Spain) (Berni et al., 2009a; Zarco-Tejada et al., 2012, 2013a,b). For this study, the UAV carried a consumer-grade camera modified in the laboratory for color-infrared (CIR) detection by removing the internal infrared filter. The camera was a Panasonic Lumix DMC-GF1 with a 4000 × 3000 pixel detector that captured images at f/3.2 and 1/2500 s with an angular FOV of 47.6° × 36.3°

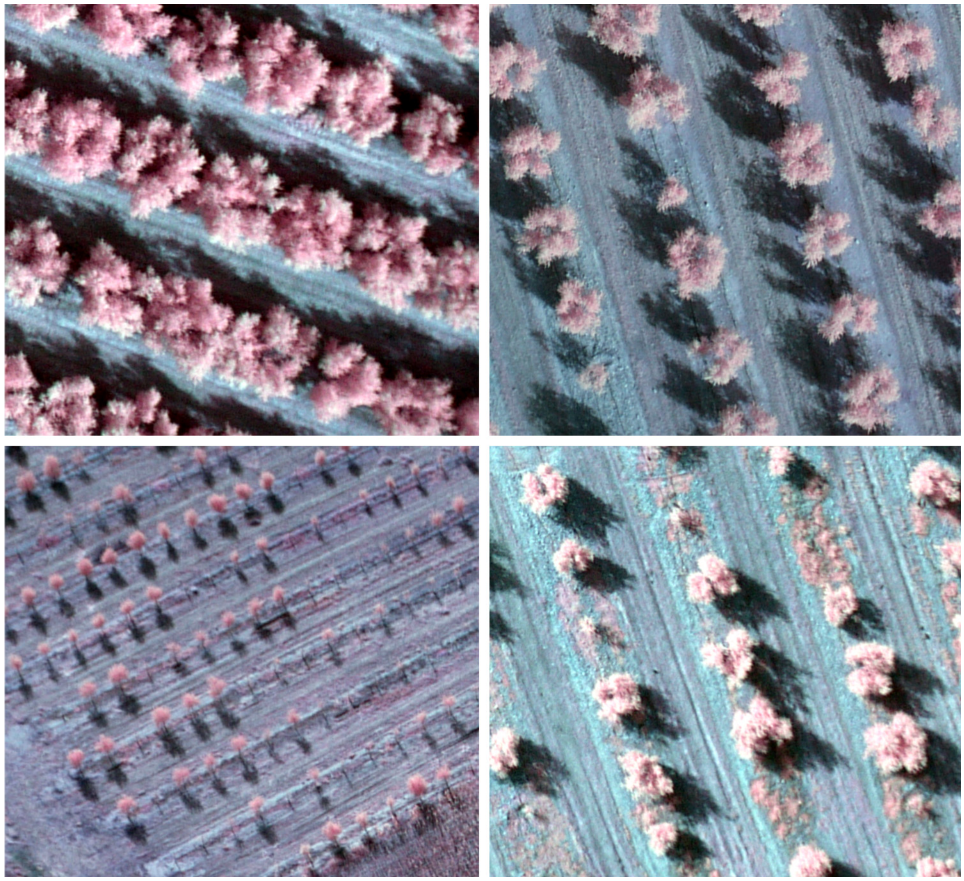

Fig. 1. Study areas flown with the UAV platform, showing a range of canopy densities and a gradient in tree crown sizes and heights as required for validation purposes. Images are provided as captured by the CIR camera, showing the NIR band in red. (For interpretation of the references to color in this figure legend, the reader is referred to the web version of the article.)

and provided ~4.5 cm pixel^{-1} resolution at an altitude of 200 m above ground level (AGL). The UAV platform used was a 2-m wingspan fixed-wing platform with up to 1-h endurance at 5.8 kg take-off weight (TOW) and 63 km/h ground speed (mX-SIGHT, UAV Services and Systems, Germany) that took 45 min to complete the entire flight plan at the indicated flight altitude. It was operated in the field by two trained operators and controlled by an autopilot for fully autonomous flying (AP04, UAV Navigation, Madrid, Spain) to follow a flight plan using waypoints to acquire imagery from the study area. The autopilot had a dual CPU controlling an integrated attitude heading reference system (AHRS) based on an L1 GPS board, 3-axis accelerometers, gyros, and a 3-axis magnetometer (Berni et al., 2009a). The ground control station and the UAV were radio linked, transmitting position, attitude, and status data at 20 Hz frequency. This tunneling transmission link was used for the operation of the cameras from the ground station deployed near the study sites. The imagery was synchronized using the GPS position and the triggering time recorded for each image. Only absolute GPS coordinates were used in this project for the generation of ortho-mosaics and DSMs, with no altitude data used as input.

The UAV platform followed two flight plans over each olive orchard (i.e. Study area 1 and Study area 2) that had been specifically designed to ensure the collection of very high resolution (VHR) imagery and large across- and along-track overlapping. The aim of this was to ensure that the photo-reconstruction method used later to derive the DSM from the VHR imagery was able to retrieve a large number of image targets allowing successful reconstruction. The area was therefore flown over using a grid of parallel and perpendicular flight lines (Fig. 2) to ensure that each ground object was imaged in the along- and across-track directions of the UAV platform, maximizing overlap. A cloud of images comprising both sets of flightlines covered the entire area homogeneously at a rate of 2 s between consecutive images, considering variations in the ground speed of the flight due to changeable wind conditions (Fig. 3a). At an average of 63 km/h ground speed, FOV = 47.6° × 36.3° and an altitude of 200 m, the resulting average overlapping obtained during the flights was extremely large and was estimated at 80–90% in most cases (Fig. 3b).

The high-resolution imagery acquired (~4.5 cm pixel^{-1}) enabled the identification of each single tree crown (Fig. 1) and a detailed assessment of branches and within-crown heterogeneity in the near-infrared spectral domain later used for validation purposes.

2.2. Generation of high-resolution DSMs

In total, 750 and 679 images from the flights conducted over both study areas were used to generate each ortho-mosaic and the digital surface model for each orchard using pix4UAV software (Ecublens, Switzerland). The processing steps included automatic aerial triangulation (AAT), bundle block adjustment (BBA), and DSM and ortho-mosaic creation. Only rough GPS tags were needed and there was no requirement for geo-location or orientation data. As the compact cameras generally used on board UAV platforms are extremely sensitive to temperature differences, vibrations, and shocks, one of the processing steps was camera auto-calibration. This involved using information from each pixel of the images to estimate the optimal camera and lens calibration for each flight.

The imagery and the synchronized GPS position for each single image were used as input. The point cloud densification was

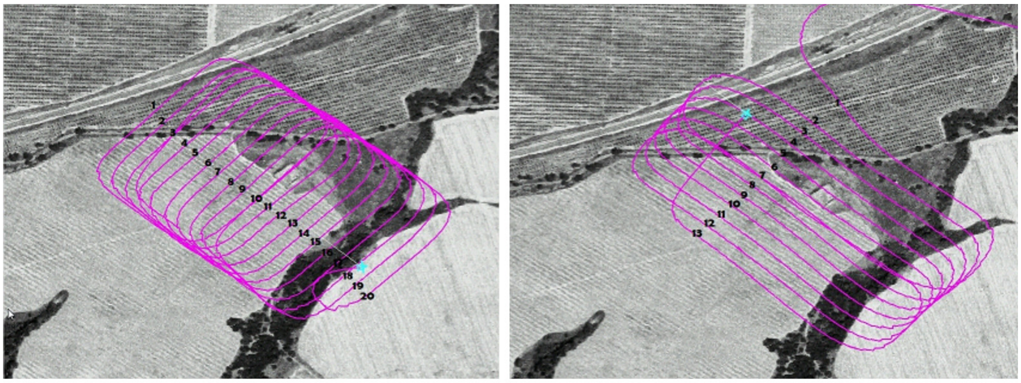

a) b)

Fig. 2. Diagram of the flight log showing the grid of east–west (a) and north–south (b) trajectories taken by the UAV platform to ensure large image overlaps.

set to high, and the grid sampling distance in the digital elevation model point cloud was set to 100 cm. The ortho-mosaic obtained had 5000 × 5000 pixel tiles with a blending factor of 0.5 and ~4.5 cm pixel^{-1} resolution, covering a total of 102 ha and 56 ha for orchards 1 and 2, respectively. The camera parameters were optimized internally during the first step conducted. The ortho-mosaic and DSM datasets obtained in this process were used to retrieve single-crown heights for each validation tree as part of the assessment conducted in the following step. The entire processing was conducted by one computer operator using a server with two 2.93 GHz processors and 48 GB RAM running with Windows Server Enterprise and a 64-bit operating system. Unattended running time for the full automatic processing was 16 h using the computer system described above.

The ortho-mosaics and DSMs were generated using the original pixel resolution (4.4–4.8 cm pixel^{-1}, resampled to 5 cm pixel^{-1}) and also after degrading the imagery through resampling to simulate pixel resolutions of 5 cm pixel^{-1} (original) and 20, 25, 30, 35, 40, and 50 cm pixel^{-1}. The objective was to simulate the effects of image resolution on the generation of DSMs and the accuracy of the tree height retrieval as a function of the input pixel size. The ultimate aim was to assess whether satellite-derived DSMs obtained from imagery with lower resolution than that acquired by low-altitude UAV platforms would enable the retrieval of tree height, assessing the error in the retrieval in such case. To this end, a total of 14 ortho-mosaics and DSMs with pixel resolutions ranging between the original 5 cm pixel^{-1} and the degraded 50 cm pixel^{-1} were generated from both study areas (7 from each). Each DSM was then co-registered using the same base map to ensure accurate registration and correct identification of the same validation trees.

As the main objective of this study was to assess the rapid processing of low-cost imagery acquired by a UAV platform using a consumer-grade camera, the ortho-mosaics and DSMs generated were obtained in a fully automated way. In the validation conducted, tree height was considered as a relative mean between the top of the crown and the ground around each tree measured. Therefore, the assessment focused on the relative integrity of the products generated rather than on the absolute errors obtained by the DSM. No ground control points (GCPs) collected in the field or user interaction were required for processing the 1429 images acquired during the UAV flight. Results of this study were therefore obtained solely based on the imagery acquired by the UAV using the Lumix camera and the associated synchronized GPS coordinates for each image. Fig. 4 shows a 3D scene obtained after the photo-reconstruction method was applied in fully automatic mode, that is, with no ground points entered in the processing steps of the ortho-mosaic and DSM generation. The trees selected for validation purposes were identified in the DSMs using this methodology, and

a) b)

Fig. 3. Location of each airborne image acquisition over the study site (a). The spatial distribution of the images acquired over the area depended on wind conditions and autopilot performance. Large overlaps are visible when the footprints of all the individual images are shown (b). At an average of 63 km/h ground speed, FOV = 47.6° × 36.3° and 200 m flight altitude, overlapping exceeded 80%.

Table 1
Summary of the images acquired over each study area, images used, mosaicked areas and pixel resolution obtained along with the outputs obtained in the bundle block adjustment in fully automatic mode.

Study area	Imagery and resolution				Bundle block adjustment		
	Images acquired	Images used	Mosaic area (ha)	GSD (cm)	Total keypoint observations	Total 3D points	Mean reprojection error (pixels)
Area 1	750	746	92.58	4.8	467,483	133,434	1.07
Area 2	679	663	56.03	4.4	287,326	81,659	1.05

the validation of tree height was conducted using the methodology described below.

2.3. Tree height validation method

A total of 152 trees were selected in the field to measure their height – 95 trees from Study area 1 and 57 trees from Study area 2. Measurements were taken with a differential Trimble R6 GPS receiver running in RTK (real-time kinematic) mode with an XY precision of 8 mm and a Z precision of 15 mm. Each measurement was taken by placing the GPS antenna at the top of the tree crown and measuring the ground coordinates around the tree as a reference. The relative mean height of each of the 152 trees measured in the field was then calculated by measuring the height and the ground level of each tree used for validation purposes. As the experiment was conducted in olive orchards, the heterogeneity of crowns was an issue due to the within-crown variability that could be observed in the field by visual inspection but also easily detected in nadir images acquired at very high resolution (Fig. 1). The high-resolution imagery used as input for DSM generation enabled the reconstruction of the within-crown heterogeneity typically observed in olive trees, with a characteristic opening at the center of the crown when observed from nadir view. This degree of detail can be observed in the DSM generated for each tree crown (Fig. 5), which enabled the reconstruction of the tree shape including features of crown heterogeneity such as crown holes and branch clumping.

Tree height was retrieved from the DSM using an approach based on the identification of local maxima likely to correspond to tree tops. First, an average filter with a 5 × 5 pixel window size (approximately 0.25 m × 0.25 m) was applied to the original DSM in order to remove both tree crown and ground artifacts. In a second stage, DSM local maxima, i.e. candidate pixels to tree tops, were identified using a square 3 m × 3 m kernel. For each of the local maxima, tree height was calculated as the difference between the minimum DSM value corresponding to the ground height and the maximum elevation corresponding to the tree top. For each of the validation trees, residuals were calculated as the difference between actual tree height measured and tree height estimated from the DSM. The root mean square error (RSME) of these residuals was calculated along with the regression fit and the squared correlation coefficient between measured and estimated tree heights; such values were assessed for each of the input pixel resolutions used in this study.

Fig. 4. 3D scene generated through photo-reconstruction methods from the consumer-grade CIR imagery acquired by the camera flown on board the UAV platform.

3. Results

3.1. Tree height quantification from the UAV-derived VHR DSM datasets

To perform the ortho-rectification and DSM generation procedure, we used 746 out of the 750 original images acquired for Study area 1, and 663 out of the 679 images acquired for Study area 2. The mosaic generated for Study area 1 covered a total of 92.58 ha, while that of Study area 2 covered 56.00 ha. The resulting ground sampling distance (GSD) of pixels was roughly the same in both areas (i.e. 4.8 and 4.4 cm pixel^{-1} in study areas 1 and 2, respectively). The bundle block adjustment process took into account 467 483 key points for Study area 1 and 287 326 points for Study area 2, using a total of 133 434 3D points and 81 659 points for the bundle block adjustment of study areas 1 and 2, respectively. In both cases, mean re-projection error was estimated at 1 pixel, approximately equivalent to 4.8 cm. A summary of these outputs for the high-resolution ortho-mosaics and DSMs generated in fully automatic mode can be seen in Table 1. A visual example of the general appearance of a subset of an entire DSM (Fig. 4) shows the 3D reconstruction including large isolated trees, orchard fields, and easily detected man-made structures.

A close-up of the trees in one of the orchards shows the 3D grid generated for each single tree (Fig. 5a and c) with the detailed surface obtained from each tree crown. When the CIR imagery was draped over the 3D grid obtained during the DSM generation process (Fig. 5b and d), the scene showed the combined near-infrared imagery and the 3D surface used for a rough validation of tree height estimation accuracy. The main issue that was visually detectable in the detailed tree-crown DSMs produced using this methodology was that the 3D surface generated for the upper part of the tree crown was visually quite good but the areas of the tree below the crown were poorly reconstructed.

The tree height data measured in the field for the total of 152 trees using the differential GPS Trimble R6 GPS receiver running in RTK mode are summarized in Table 2. The tree heights selected for the validation ranged between 1.16 m and 4.38 m, with a mean height of 3.08 m and 2.97 m for study areas 1 and 2, respectively. The quantitative analysis aimed at assessing the accuracy of tree height retrieval was conducted for each of the two areas separately

Table 2
Summary of tree height data measured in the field over each study site for the total of 152 trees using a differential GPS running in RTK mode.

Study area	N	T_{height} (min) (m)	T_{height} (max) (m)	T_{height} (mean) (m)
Area 1	95	1.16	4.38	3.08
Area 2	57	1.76	4.22	2.97

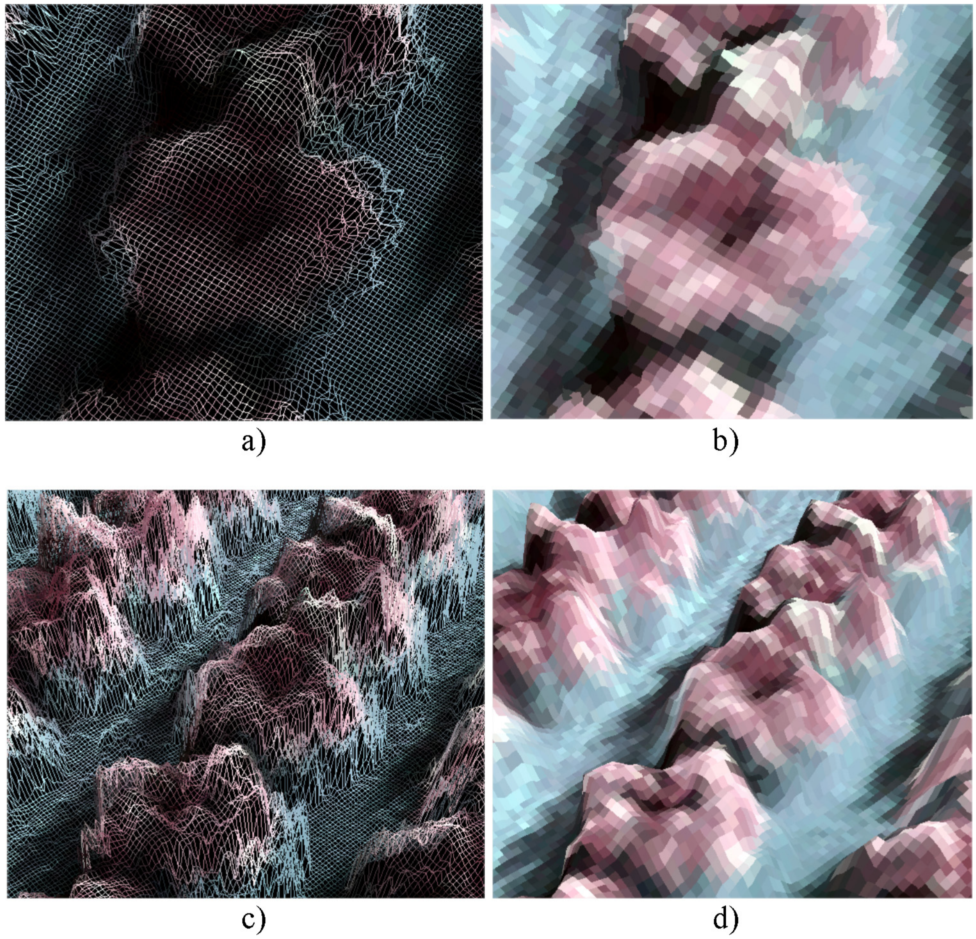

Fig. 5. The single tree photo-reconstruction (a) and (c) obtained from the UAV imagery with the ortho-mosaic draped over the DSM (b) and (d) shows the within-crown heterogeneity observed in trees. The VHR DSMs calculated for each validation tree were used to assess tree height quantification accuracy.

and also for both areas together. The reason for such combined and area-independent analysis was that the imagery was acquired for both study areas during the same flight and therefore under the same conditions, but the mosaics and DSMs were generated separately for each study area because there was no overlapping between areas.

Results of the validation work that consisted of comparing field-measured tree height to DSM-retrieved height for each of the 152 validation trees distributed over the two study areas can be seen in Fig. 6. Results show coefficients of determination above 0.8 both when the study areas were assessed separately (R^2 = 0.86 for Study area 1; R^2 = 0.81 for Study area 2) and when both areas were merged together (R^2 = 0.83). Relative root mean square error (R-RMSE) ranged between 10% and 13% depending on the study area, that is, an R-RMSE = 10.8% (Study area 1), an R-RMSE = 13.3% (Study area 2), and an R-RMSE = 11.5% when both areas were assessed together. In terms of actual dimensions, these R-RMSE values indicated root mean square errors (RMSE) below 40 cm, that is, an RMSE = 33 cm (Study area 1), an RMSE = 39 cm (Study area 2), and a combined RMSE = 35 cm when both areas were assessed together.

3.2. Spatial resolution effects on DSM generation and tree height quantification

The assessment of the effects of image resolution on DSM generation was performed using the original dataset (5 cm pixel^{-1} size) and comparing it to the surface models developed with 20, 25, 30, 35, 40, and 50 cm pixel^{-1} image resolution. The resulting effects regarding pixel resolution (Fig. 7) clearly show a loss of detail when the input images used for DSM generation were degraded from the original 5 cm pixel^{-1} resolution (Fig. 7a) to 50 cm pixel^{-1} size (Fig. 7d). Results show a loss of within-crown heterogeneity due to the lower spatial resolution obtained, with an effect on 3D surfaces (Fig. 7). As expected, the details observed in the DSM obtained using 5 cm pixel^{-1} input images (Fig. 7e and g) were lost in the surface model obtained with 50 cm pixel^{-1} resolution (Fig. 7f and h). This had implications for the retrieval of tree height and the errors obtained.

The coefficients of determination obtained for tree height estimation as a function of the spatial resolution of the imagery used as input for DSM generation can be seen in Fig. 8a. Results showed that the coefficient of determination decreased to R^2 = 0.5 when the input images used for the DSM had 50 cm pixel^{-1} resolution, while the results obtained with the original 5 cm pixel^{-1} imagery yielded R^2 = 0.86. More interestingly, relationships started to degrade in this particular study once image pixel size was greater than 35 cm pixel^{-1}. Input images with 20 cm pixel^{-1} resolution only weakened the relationship from R^2 = 0.86 to R^2 = 0.81. This result is of particular interest considering that, for this application focused on tree height quantification, results suggest that extremely high image resolution (5 cm pixel^{-1}) may not be needed. The main advantage of this is that larger areas can be covered by UAV platforms if the target pixel resolution is in the range of 20–30 cm pixel^{-1}. In fact, the relationship between estimated and measured tree heights still held (Fig. 9a) at 35 cm pixel^{-1} image resolution, yielding R^2 = 0.78 and a relationship close to the 1:1 line.

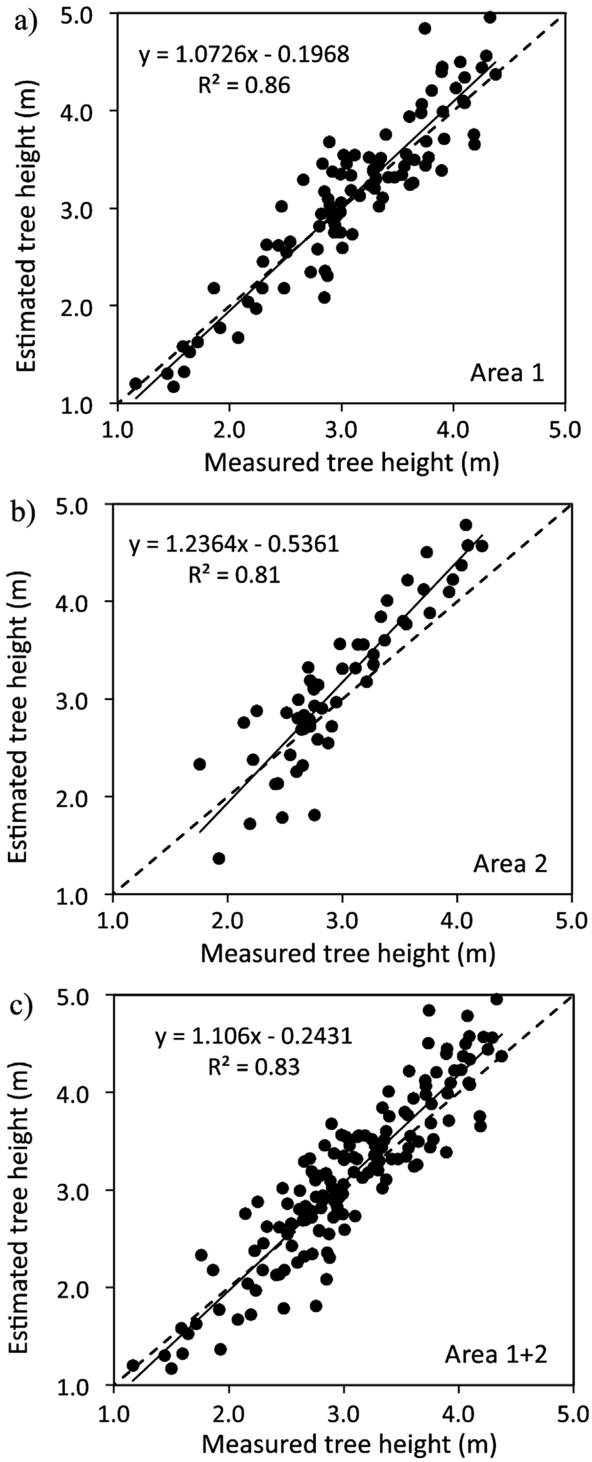

Fig. 6. Results of the validation assessment comparing field-measured tree height and DSM-retrieved height for each of the 152 validation trees distributed over Study area 1 (a), Study area 2 (b), and both areas combined (c). The dashed line represents the 1:1 line, and the solid line represents the fitted linear function. Parameters of the linear regression and coefficient of determination are given in each plot.

The relationship weakened (R^2 = 0.5) at lower spatial resolution and started to deviate from the 1:1 distribution due to large errors in some of the validation trees measured in the field (Fig. 9b). The relationship obtained with 35 cm pixel^{-1} image resolution (Fig. 9a) (R^2 = 0.78) was close to that obtained with the original 5 cm pixel^{-1} image resolution (Fig. 6a) (R^2 = 0.86), with small effects due to image degradation.

The effects of image resolution on the RMSE and R-RMSE obtained can be seen in Fig. 8b and c, respectively. The RMSE obtained with the original 5 cm pixel^{-1} imagery (33 cm) degraded up to 60 cm when image resolution reached 50 cm pixel^{-1} size. The error obtained was 38 cm at 20 cm pixel^{-1} resolution and increased to 42 cm at 35 cm pixel size. Large errors were obtained when image resolution reached 40 cm, yielding 58 cm RMSE. As regards the R-RMSE values obtained, the original 10.8% error at 5 cm pixel^{-1} resolution increased to 19.3% when 50 cm pixel^{-1} resolution imagery was used to generate the DSM. In the 5–35 cm pixel^{-1} range, the errors obtained ranged between 10.8% and 14%, the latter obtained with 30 cm pixel^{-1} resolution imagery. Although the coefficients of determination were not greatly affected when 5 cm pixel^{-1} imagery was degraded to 30–35 cm pixels (i.e. R^2 decreased from 0.86 to 0.75), the actual effects on the RMSE and R-RMSE values obtained could be considered high: when resolution changed from 5 to 30 cm pixel^{-1}, RMSE degraded from 33 to 43 cm, indicating an R-RMSE degradation between 10.8% and 14%.

4. Discussion

Some studies have provided good examples of 3D reconstructions and VHR DSMs obtained for different applications. However, to the best of our knowledge, no quantitative validations of vegetation height have been reported or published so far specifically regarding crop trees for use in agronomy, plant breeding, or other agricultural applications. Results obtained in this study on tree height quantification using a low-cost consumer-grade CIR camera are comparable to canopy height estimates obtained with airborne laser scanner technology from vegetation canopies. The estimation error (35 cm RMSE, 11.5% R-RMSE) quantified for tree heights with a range of variation between 1.16 and 4.38 m (R^2 = 0.83) was obtained with a low-cost camera on board a lightweight UAV platform (i.e. under 6 kg TOW) using fully automatic processing without field ground control points. These results are comparable to those obtained for tree height quantification from airborne laser scanners (ALS) and reported in various experiments conducted on this same topic (i.e. errors ranging between 0.09 m and 1.2 m depending on canopy type and phenological phase) (Kaartinen et al., 2012; Ma et al., 2012; Edson and Wing, 2011; Pirotti, 2010; Tesfamichael et al., 2010a,b; Gratziolis et al., 2010). The main disadvantage of the methodology reported in this manuscript is that canopy height quantification was conducted on a relative basis. Therefore, the errors obtained in absolute coordinates would need to be reduced using ground control points to improve the absolute accuracy of the DSMs generated.

The main advantage of the fully automated methods used here is that no user interaction was required during the image processing stage and no data collection in the field was needed to obtain such accuracies. Nevertheless, some applications may require more accurate results in absolute means, and this low-cost approach would therefore require the collection of some field targets to ensure this. In this study, focused on open canopies where the top of the canopy and the background level were easy to identify, the low-cost solution based on fully automatic procedures demonstrated its validity for assessing canopy height, with future potential for crown volume estimates considering the large canopy detail observed in the 3D reconstruction of the trees. For this method to be successful, the canopy should be open enough to allow for the identification of ground points at the base of the trees. This is the case of heterogeneous canopies, orchards, and open crops characterized by a discontinuous architecture in which the pure vegetation and soil components can be identified if very high resolution imagery is used (i.e. from centimeter up to half-meter resolution). This study also shows the applicability of the method for identifying and

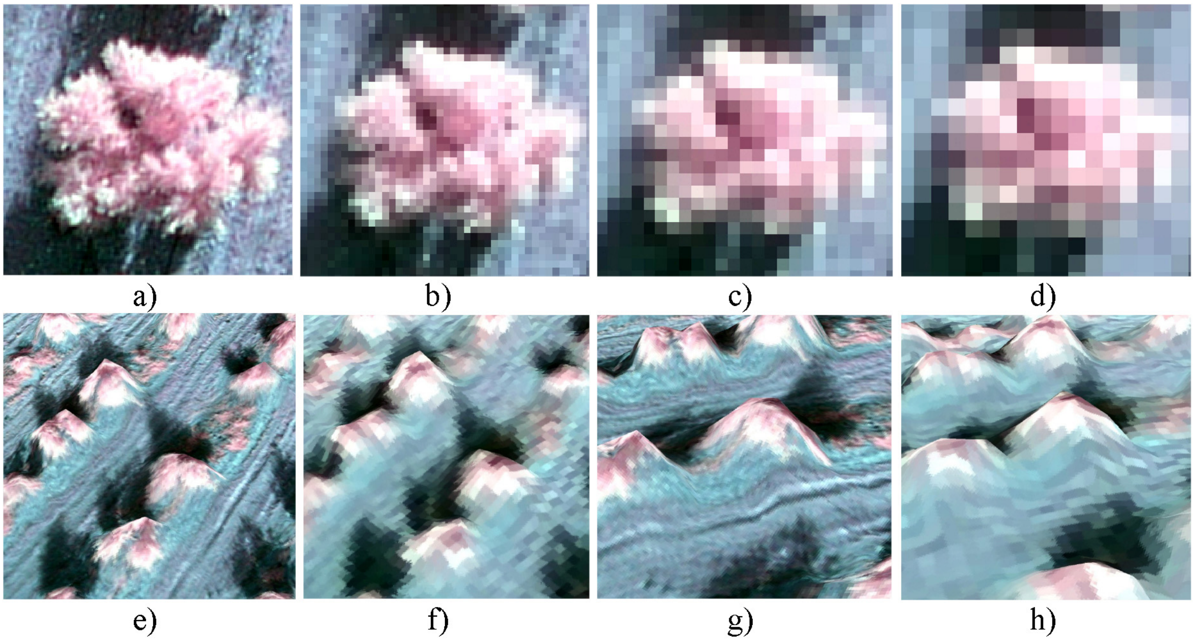

Fig. 7. Image degradation from the original 5 cm pixel^{-1} resolution (a) to 20 cm pixel^{-1} (b), 25 cm pixel^{-1}, 30 cm pixel^{-1}, 35 cm (c), 40 cm pixel^{-1}, and 50 cm pixel^{-1} used for the DSM accuracy assessment. The image resolution showed visual effects generated on the DSMs from the original 5 cm pixel^{-1} resolution imagery (e) and (g) and the 50 cm pixel^{-1} resolution imagery (f) and (h).

monitoring certain types of landscape features in agricultural landscapes (i.e. hedges or tress that are isolated, clumped or arranged in rows) in the framework of EU CAP implementation. In fact, such landscape features are generally characterized as protruding vegetation elements in a matrix with an even (and normally low) crop layer that allows an easy retrieval of reference ground or in this case crop canopy level points.

A potential disadvantage of this methodology is the high overlapping and the low altitude requirements of UAV flights. The very high resolution imagery acquired with such lightweight UAVs limits the areas flown over to a few hundred hectares in one single flight at the most. This problem can be overcome with higher resolution cameras flying at higher altitudes to improve efficiency. As an example, it took 45 min to cover 150 ha in one single flight with the UAV used in this experiment, but the same area could have been covered in only 15 min if the UAV had been flown at 600 m AGL. At that altitude, the spatial resolution would still be acceptable for this application using the same camera, which would deliver 15 cm pixel resolution. In addition, available UAVs with longer endurance can enable the acquisition of larger areas, but legal and operational issues depending on the country may also be a limitation. It is generally accepted that the technology presented in this manuscript is capable of covering up to thousands of hectares at the most, which is a limitation when larger coverage (i.e. hundreds of thousands of hectares) is required for the global monitoring of larger areas. Nevertheless, the methodologies presented here can be readily applicable to manned airborne platforms carrying the same low-cost camera payloads, obtaining similar (if not better) results with longer endurance capabilities and acquiring larger areas in a single flight without legal limitations.

Regardless of the platform used to carry the low-cost camera payloads used in this study, this low-cost approach makes it possible to obtain accurate DSMs in a much simpler way than using the complex LIDAR systems that are currently operational. The intention is not to start a debate on the performance of each of these technologies, as studies have already proven the many advantages of airborne laser scanners for assessing canopy structure and building realistic 3D scene representations of canopy architecture with unprecedented accuracy and detail (Lefsky et al., 1999; Lovell et al., 2003; Drake et al., 2002; Coops et al., 2007; Parker et al., 2004; Wang et al., 2008). It is the cost of the sensor (i.e. LIDAR vs. consumer-grade RGB or CIR camera) and the ease of operation and processing of consumer-grade cameras that makes this new technology of high interest and potential for the scientific community and customers interested in the monitoring of vegetation dynamics, crop assessments, landscape feature identification, and erosion studies, among others. Although miniaturized LIDAR systems on board lightweight UAVs are starting to be operational, their cost and operation and the processing complexity of the data obtained prevent their wide use for applications and uses such as that described in this paper. Several successful examples of the use of LIDAR sensors on board low-cost UAV platforms for canopy characterization have already demonstrated a very high potential. An example is the use of a lightweight LIDAR system on board a multicopter platform that yielded up to 62 points per square meter and tree height quantification errors ranging between 15 and 26 cm. Nevertheless, certain issues need to be considered when low-density clouds are obtained from miniaturized LIDAR systems because previous work has shown that tree height tends to be underestimated due to a large probability of missing treetops even with high point-sampling densities (Yu et al., 2004; Chen et al., 2006). In addition, the heavier weight of miniaturized LIDAR sensors as compared to low-cost RGB and CIR cameras requires larger UAVs for their operation, generally based on rotary platforms such as multicopters or helicopters, which cover very small areas due to the low speed of the platform and the heavy payloads carried. For this reason, these systems generally yield only a few hectares per flight, which is a serious limitation for the operational use of miniaturized LIDAR systems on board UAV platforms.

Future work should focus on improving the absolute accuracy of the DSMs obtained through the methodology presented in this manuscript and assessing other discontinuous crop canopies of commercial interest (i.e. vineyards and citrus plantations) in which canopy parameters such as crown height and volumes are of

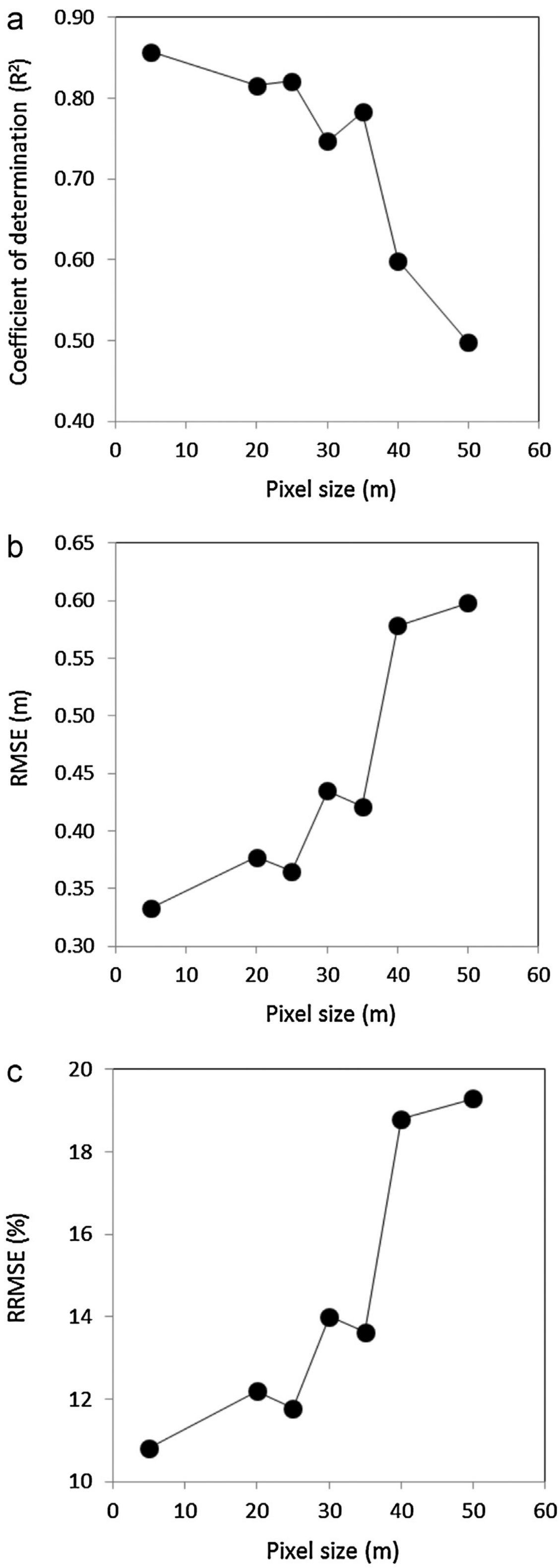

Fig. 8. Coefficients of determination (R^2) (a), RMSE (b), and R-RMSE (c) obtained for the tree height estimation assessment conducted from DSMs generated for different input spatial resolutions.

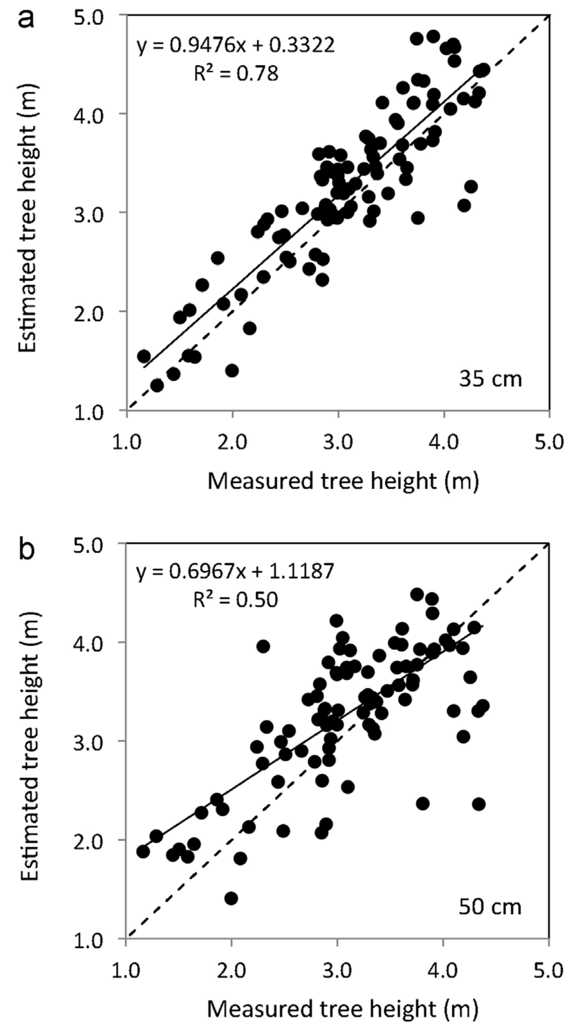

Fig. 9. Tree height quantification results obtained from 35 cm pixel^{-1} input imagery (a) as compared to 50 cm pixel^{-1} resolution imagery (b) and as obtained from the original 5 cm pixel^{-1} image resolution imagery (Fig. 6a).

interest for agronomic purposes. Additionally, use of these cost-efficient cameras on board UAV platforms opens a whole new avenue of possibilities due to the rapid development of miniaturized cameras with multispectral, thermal, and hyperspectral capabilities. For the purpose of pure quantitative remote sensing objectives, multi-lense cameras with narrow-band filters and hyperspectral cameras with hundreds of narrow bands are better suited to monitor vegetation condition and physiological stress. The main reason for this is that such cameras target certain narrow bands directly associated with specific absorption features related to chlorophyll and other pigments as well as canopy density and LAI. Nevertheless, the type of consumer-grade camera used in this study can be used to derive biophysical parameters if the purpose is to calculate pseudo-NDVI images that may be related to vegetation canopy structural characteristics. Radiometric calibration and atmospheric correction methods (i.e. to account for downwelling irradiance at the time of flights) should be implemented for such quantitative remote sensing purposes. In fact, methodologies are currently available and some studies have already shown successful results.

The application of this methodology for European-level landscape feature identification from satellite-derived DSMs should be explored in the context of the European Common Policy, assessing the potential of these methods for covering large areas.

5. Conclusions

This study represents progress in the assessment of canopy height in a discontinuous crop canopy using digital surface models obtained from very high resolution imagery acquired with an unmanned aerial vehicle. It demonstrates that a consumer-grade camera on board a low-cost unmanned platform generated 3D scenes of an area covering 150 ha at 5 cm pixel^{-1} resolution that were used to quantify single-tree heights with a fully automatic method requiring minimal human intervention. The two study areas, whose surface was 92 ha and 56 ha, respectively, were flown over with the UAV platform using a pre-defined flight plan to ensure large overlaps exceeding 80% in both along- and across-track directions. The very high resolution imagery acquired on both sites (i.e. a total of 750 and 679 images, respectively) was able to generate ortho-mosaics and DSMs for each site at 5 cm pixel^{-1} resolution. The validation performed by measuring 152 trees in the field with a RTK GPS system demonstrated the following errors in the estimation of tree height: RMSE = 35 cm and R-RMSE = 11.5% in trees with a range of variation between 1.16 and 4.38 m, yielding R^2 = 0.83. Additionally, the assessment conducted to evaluate the effects of the spatial resolution of the input images on the DSMs generated demonstrated the stability of relationships obtained when pixel resolution was within the range of 5 and 30 cm pixel^{-1}. Yet, relationships rapidly degraded for input images with pixel resolutions below 35 cm. RMSE and R-RMSE values obtained as a function of input pixel resolution demonstrated that errors below 15% were obtained when 30 cm pixel^{-1} resolution imagery was used to generate the DSMs. This study highlights that an inexpensive approach based on consumer-grade cameras on board a hand-launched unmanned system can provide similar accuracies to those of the more complex and costly LIDAR systems currently operated for agricultural and environmental applications.

Acknowledgments

The Institute for Sustainable Agriculture (IAS) of the Spanish Council for Scientific Research (CSIC) is acknowledged for sharing the UAV airborne datasets required for the analysis. A. Gomez, D. Notario, A. Vera, A. Hornero, and R. Romero (QuantaLab-IAS-CSIC research laboratory) are acknowledged for their contribution during the airborne and field campaigns.

References

Berni, J.A.J., Zarco-Tejada, P.J., Suárez, L., Fereres, E., 2009a. Thermal and narrow-band multispectral remote sensing for vegetation monitoring from an unmanned aerial vehicle. IEEE Transactions on Geoscience and Remote Sensing 47 (3), 722–738.

Berni, J.A.J., Zarco-Tejada, P.J., Sepulcre-Cantó, G., Fereres, E., Villalobos, F.J., 2009b. Mapping canopy conductance and CWSI in olive orchards using high resolution thermal remote sensing imagery. Remote Sensing of Environment 113, 2380–2388.

Bork, E.W., Su, J.G., 2007. Integrating LIDAR data and multispectral imagery for enhanced classification of rangeland vegetation: a meta analysis. Remote Sensing of Environment 111, 11–24.

Chen, Q., Baldocchi, D., Gong, P., Kelly, M., 2006. Isolating individual trees in a savanna woodland using small footprint LIDAR data. Photogrammetric Engineering and Remote Sensing 72 (8), 923–932.

Chopping, M., Moisen, G., Su, L., Laliberte, A., Rango, A., Martonchik, J.V., 2008. Large area mapping of south western forest crown cover, canopy height, and biomass using MISR. Remote Sensing of Environment 112, 2051–2063.

Coops, N.C., Hilker, T., Wulder, M.A., 2007. Estimating canopy structure of Douglas-fir forest stands from discrete-return LIDAR. TREES-Structure and Function 21 (3), 295–310.

Drake, J.B., Dubayah, R.O., Knox, R.G., 2002. Sensitivity of large-footprint LIDAR to canopy structure and biomass in a neotropical rainforest. Remote Sensing of Environment 81 (2–3), 378–392.

Edson, C., Wing, M.G., 2011. Airborne light detection and ranging (LIDAR) for individual tree stem location, height, and biomass measurements. Remote Sensing 3 (11), 2494–2528.

González-Dugo, V., Zarco-Tejada, P.J., Berni, J.A., Suárez, L., Goldhamer, D., Fereres, E., 2012. Almond tree canopy temperature reveals intra-crown variability that is water stress-dependent. Agricultural and Forest Meteorology 154–155, 156–165.

Gratziolis, D., Fried, J.S., Monleon, V.S., 2010. Challenges to estimating tree height via LIDAR in closed-canopy forests: a parable from Western Oregon. Forest Science 56 (2), 139–155.

Guillén-Climent, M.L., Zarco-Tejada, P.J., Berni, J.A.J., North, P.R.J., Villalobos, F.J., 2012. Mapping radiation interception in row-structured orchards using 3D simulation and high resolution airborne imagery acquired from a UAV. Precision Agriculture 13, 473–500.

James, M.R., Robson, S., 2012. Straightforward reconstruction of 3D surfaces and topography with a camera: accuracy and geoscience application. Journal of Geophysical Research: Earth Surface 117, F03017.

Kaartinen, H., Hyyppä, J., Yu, X., Vastaranta, M., Hyyppä, H., Kukko, A., Holopainen, M., Heipke, C., Hirschmugl, M., Morsdorf, F., Næsset, E., Pitkänen, J., Popescu, S., Solberg, S., Wolf, B.M., Wu, J.-C., 2012. An international comparison of individual tree detection and extraction using airborne laser scanning. Remote Sensing 4 (4), 950–974.

Küng, O., Strecha, C., Beyeler, A., Zufferey, J.-C., Floreano, D., Fua, P., Gervaix, F., 2011. The accuracy of automatic photogrammetric techniques on ultra-light UAV imagery. ISPRS – International Archives of the Photogrammetry, Remote Sensing and Spatial Information Sciences XXXVIII-1, 125–130.

Lefsky, M.A., Cohen, W.B., Acker, S.A., 1999. LIDAR remote sensing of the canopy structure and biophysical properties of Douglas-fir western hemlock forests. Remote Sensing of Environment 70 (3), 339–361.

Lovell, J.L., Jupp, D.L.B., Culvenor, D.S., 2003. Using airborne and ground-based ranging LIDAR to measure canopy structure in Australian forests. Canadian Journal of Remote Sensing 29 (5), 607–622.

Ma, H., Song, J., Wang, J., Yang, H., 2012. Comparison of the inversion ability in extrapolating forest canopy height by integration of LIDAR data and different optical remote sensing products. In: Geoscience and Remote Sensing Symposium (IGARSS), 2012 IEEE International, Munich, 22–27 July 2012, pp. 3363–3366, ISSN: 2153-6996.

Parker, G.G., Harding, D.J., Berger, M.L., 2004. A portable LIDAR system for rapid determination of forest canopy structure. Journal of Applied Ecology 41 (4), 755–767.

Pirotti, F., 2010. Assessing a template matching approach for tree height and position extraction from LIDAR-derived canopy height models of *Pinus pinaster* stands. Forests 1 (4), 194–208.

Rouse, J.W., Haas, R.H., Schell, J.A., Deering, D.W., Harlan, J.C., 1974. Monitoring the vernal advancements and retrogradation of natural vegetation. In: MD, U.G. (Ed.), NASA/GSFC Final Report. , p. 371.

Selkowitz, D.J., Green, G., Peterson, B., Wylie, B., 2012. A multisensor LIDAR, multi-spectral and multi-angular approach for mapping canopy height in boreal forest regions. Remote Sensing of Environment 121 (1), 458–471.

Strecha, C., von Hansen, W., Van Gool, L., Fua, P., Thoennessen, U., 2008. On benchmarking camera calibration and multi-view stereo for high resolution imagery. In: IEEE Computer Vision and Pattern Recognition, CVPR 2008, Anchorage, AK, 23–28 June 2008, pp. 1063–6919.

Suárez, L., Zarco-Tejada, P.J., González-Dugo, V., Berni, J.A.J., Sagardoy, R., Morales, F., Fereres, E., 2010. Detecting water stress effects on fruit quality in orchards with time-series PRI airborne imagery. Remote Sensing of Environment 114, 286–298.

Takahashi, M., Shimada, M., Tadono, T., Watanabe, M., 2012. Calculation of tree height using PRISM-DSM. In: Geoscience and Remote Sensing Symposium (IGARSS), 2012 IEEE International, Munich, 22–27 July 2012, pp. 6495–6498, ISSN: 2153-6996.

Tesfamichael, S.G., van Aardt, J.A.N., Ahmed, F., 2010a. Estimating plot-level tree height and volume of *Eucalyptus grandis* plantations using small-footprint, discrete return LIDAR data. Progress in Physical Geography 34 (4), 515–540.

Tesfamichael, S.G., Ahmed, F., van Aardt, J.A.N., 2010b. Investigating the impact of discrete-return LIDAR point density on estimations of mean and dominant plot-level tree height in *Eucalyptus grandis* plantations. International Journal of Remote Sensing 31 (11), 2925–2940.

Vallet, J., Panissod, F., Strecha, C., Tracol, M., 2011. Photogrammetric performance of an ultra light weight swinglet "UAV". In: International Archives of the Photogrammetry, Remote Sensing and Spatial Information Sciences, vol. XXXVIII-1/C22, ISPRS Zurich 2011 Workshop, 14–16 September 2011, Zurich, Switzerland.

Wallerman, J., Bohlin, J., Fransson, J.E.S., 2012. Forest height estimation using semi-individual tree detection in multi-spectral 3D aerial DMC data. In: Geoscience and Remote Sensing Symposium (IGARSS), 2012 IEEE International, Munich, 22–27 July 2012, pp. 6372–6375, ISSN: 2153-6996.

Wang, Y., Weinacker, H., Koch, B., 2008. A LIDAR point cloud based procedure for vertical canopy structure analysis and 3D single tree modelling in forest. Sensors 8 (6), 3938–3951.

Waser, L.T., Baltsavias, E., Ecker, K., Eisenbeiss, H., Ginzler, C., Kuchler, M., Thee, P., Zhang, L., 2008. High-resolution digital surface models (DSMs) for modeling fractional shrub/tree cover in a mire environment. International Journal of Remote Sensing 29 (5), 1261–1276.

Yu, X., Hyyppä, J., Kaartinen, H., Maltamo, M., 2004. Automatic detection of harvested trees and determination of forest growth using airborne laser scanning. Remote Sensing of Environment 90 (4), 451–462.

Zarco-Tejada, P.J., Berni, J.A.J., Suárez, L., Sepulcre-Cantó, G., Morales, F., Miller, J.R., 2009. Imaging chlorophyll fluorescence from an airborne narrow-band

multispectral camera for vegetation stress detection. Remote Sensing of Environment 113, 1262–1275.
Zarco-Tejada, P.J., González-Dugo, V., Berni, J.A.J., 2012. Fluorescence, temperature and narrow-band indices acquired from a UAV platform for water stress detection using a micro-hyperspectral imager and a thermal camera. Remote Sensing of Environment 117, 322–337.
Zarco-Tejada, P.J., Guillén-Climent, M.L., Hernández-Clemente, R., Catalina, A., González, M.R., Martín, P., 2013a. Estimating leaf carotenoid content in vineyards using high resolution hyperspectral imagery acquired from an unmanned aerial vehicle. Agricultural and Forest Meteorology 171–172, 281–294.
Zarco-Tejada, P.J., Morales, A., Testi, L., Villalobos, F.J., 2013b. Spatio-temporal patterns of chlorophyll fluorescence and physiological and structural indices acquired from hyperspectral imagery as compared with carbon fluxes measured with eddy covariance. Remote Sensing of Environment 133, 102–115.